analytical chemistry

ARTICLE

pubs.acs.org/ac

Plasmonic Properties of the Multispot Copper-Capped Nanoparticle Array Chip and Its Application to Optical Biosensors for Pathogen Detection of Multiplex DNAs

Do-Kyun Kim,[†] Seung Min Yoo,[†,#] Tae Jung Park,[*,†,‡] Hiroyuki Yoshikawa,[§] Eiichi Tamiya,[§] Jung Youn Park,[⊥] and Sang Yup Lee[*,†,#]

[†]BioProcess Engineering Research Center, Center for Systems & Synthetic Biotechnology, and Institute for the BioCentury, KAIST, 291 Daehak-ro, Yuseong-gu, Daejeon 305-701, Republic of Korea

[‡]Center for Nanobio Integration & Convergence Engineering, National Nanofab Center, 291 Daehak-ro, Yuseong-gu, Daejeon 305-806, Republic of Korea

[§]Department of Applied Physics, Graduate School of Engineering, Osaka University, 2-1 Yamadaoka, Suita, Osaka 565-0871, Japan

[⊥]Biotechnology Research Division, National Fisheries Research & Development Institute (NFRDI), 408-1 Sirang-ri, Gijang, Busan 619-705, Republic of Korea

[#]Department of Chemical & Biomolecular Engineering (BK21), Department of Bio & Brain Engineering, Department of Biological Sciences, and Bioinformatics Research Center, KAIST, 291 Daehak-ro, Yuseong-gu, Daejeon 305-701, Republic of Korea

Supporting Information

ABSTRACT: A localized surface plasmon resonance (LSPR)-based optical biosensor in connection with a multispot copper-capped nanoparticle array (MC-NPA) chip was proposed and developed. The copper (Cu) films, used as a shell, formed a "cap-like" layer on the top of the silica nanoparticles, used as a core, in an orderly fashion, to form the surface called a "Cu-capped nanoparticle array chip". The plasmonic properties of this nanostructure type were initially investigated while controlling the shell thickness of the deposited Cu. Also, we quantified the sensitivity of MC-NPA chip to changes in bulk refractive index (RI). As a result of its LSPR properties, the MC-NPA chip displayed a sensitivity of 67.8 nm per RI unit, and the wavelength shift of the LSPR spectrum peak was sensitive to the RI of the surrounding bulk medium, such as the biomolecular layers. Using MC-NPA chips, multiplex sensing of target DNAs from reference bacteria and clinical samples was possible in a quantitative manner with a detection limit of 10 fM (50 zmol). The optical biosensor developed in this study represents a unique approach to performing LSPR that utilizes a simple and cost-effective optical setup with disposable chips.

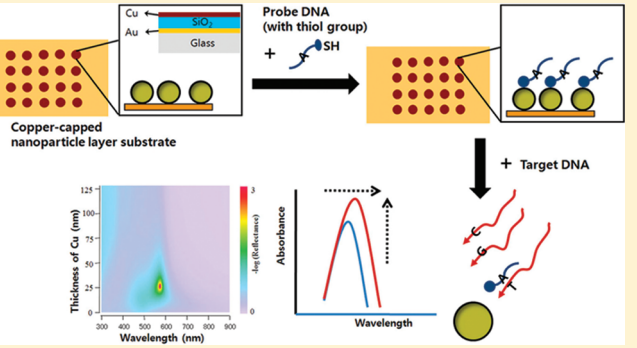

In recent years, metallic nanostructures have become an interesting topic for many researchers because of their specific optical characteristics. The collective charge density oscillations of nanostructures are defined as localized surface plasmon resonance (LSPR). The LSPR is excited when electromagnetic radiation of incident light interacts with the free electrons of the nanostructures, which results in collective oscillations, leading to strong enhancements of the local electromagnetic fields surrounding the nanostructures.[1−3] Depending on the types of materials, sizes, and shapes of nanostructures, LSPR spectrum peaks have various sensing capacities for the interfacial refractive index (RI) and biomolecular interactions.[4−7]

Metallic nanoshells, spherical nanoparticles (NPs) composed of a dielectric core and a concentric metal shell, are NPs whose plasmon resonant energies are particularly sensitive to geometry.[8] Coinage metallic nanoshells such as gold (Au) and silver (Ag) have been of particular interest for LSPR properties because they can support NP plasmon resonance in the ultraviolet, visible, and near-infrared regions of the spectrum, modifiable by varying NP size and shape.[9−14] In core−shell type optical device applications, copper (Cu) may potentially be desirable over Au or Ag because of its compatibility with dielectric core-based processing.[15] Moreover, Cu nanoshells are of significant interest for potential large-scale or large-area applications relative to their Au and Ag counterparts because of the significantly reduced relative cost of the constituent metal. However, Cu is

Received: March 28, 2011
Accepted: June 29, 2011
Published: June 29, 2011

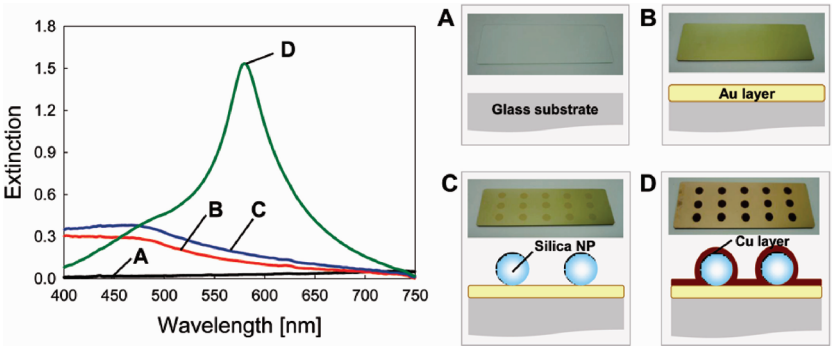

Figure 1. LSPR optical characteristics and fabrication procedure of the MC-NPA chip (A) slide glass substrate, (B) after Au deposition on the slide glass substrate, (C) after immobilization of the silica NP layer on the Au-deposited slide glass substrate, and (D) after Cu deposition on the silica NP layer. The LSPR spectrum peak of the MC-NPA chip was observed at 580 nm.

unstable, difficult to work with, and prone to surface oxidation that can significantly affect the optical properties. Cu is prone to surface oxidation upon exposure to ambient laboratory atmosphere at room temperature (RT). As a result of surface oxidation, the plasmonic properties of Cu have not received much attention as compared to Au and Ag.

To overcome the problems associated with the surface oxidation of Cu metal, many researchers have implemented continuously in order to fabricate the Cu-based optical device. Sinha and co-workers reported the preparation of Cu NPs in an aqueous medium with hydrazine hydrate as a reductant.[16] Various stabilizers such as polyvinyl alcohol (PVA), polyvinyl pyrolidone (PVP), and starch have been considered. The effect of concentration of NaOH on the synthesis of Cu NPs has been investigated. However, the growth mechanisms of Cu nanocrystals and Cu NPs are not well established yet because it has been difficult to prevent coalescence. Nanocrystals and NPs have to be coated during and after the formation process, and it is difficult to determine the effect of passivation agents on the structure. Van Duyne and co-workers reported the LSPR properties of oxide-free Cu NPs fabricated by nanosphere lithography.[17] The LSPR properties of the Cu NPs were significantly affected by the presence of Cu oxides, and the removal of the oxide species with glacial acetic acid yields a dramatic difference in the observed LSPR spectra.

In this report, we focused our attention on the fabrication of multispot copper-capped nanoparticle array (MC-NPA) chips and their application to an LSPR-based label-free optical biosensor. Different from the fabrication of Cu NPs and/or Cu nanocrystals in solution, Cu-capped NP structures are easily controlled in various formats with high reproducibility and possess a stable optical extinction response under ambient temperatures. In the construction of MC-NPA, the silica NPs were used as the core, and thin Cu films were used as the shell coating at the top of the core. Therefore, we monitored the increase in the extinction intensity following the coating of 100 nm on silica NPs with controlled layers of Cu. Here, we present our MC-NPA chip as a suitable platform to monitor the alteration in the LSPR properties caused by various thicknesses of the Cu layer. Also, we investigate the ability of the Cu layer to transduce changes in the surrounding RI into the LSPR spectrum. As a result, the MC-NPA chip gives a sensitivity of 67.8 nm per RI unit (RIU). This MC-NPA chip was readily applicable to label-free optical biosensors as a rapid and user-friendly alternative to conventional techniques. This is the first report on the monitoring of DNA hybridization by using dense NP array chips based on a Cu metal substrate. In order to eliminate the influence of the Cu oxide layer on the MC-NPA chip surface, a Cu oxide removal procedure was implemented by using acetic acid. Using the MC-NPA chips, target DNAs from the reference strain and clinical samples can identify with ultrasensitivity (detection limit of 10 fM (50 zmol)) and high specificity in a quantitative manner, indicating that the plasmonic characteristic of the chips is shown to be highly sensitive to the biomolecular layer thickness. The LSPR-based optical biosensor in connection with a MC-NPA chip is easy to fabricate. The apparatus cost for the evaluation of optical properties is lower than that for conventional SPR apparatus, and the procedure has become more convenient without labeling. Furthermore, this MC-NPA chip could detect a low concentration of target DNA.

EXPERIMENTAL SECTION

Fabrication Process of the MC-NPA Chip. Figure 1 shows the LSPR optical characteristics and fabrication procedure of the MC-NPA chip. For the deposition of Au on the slide glass substrate (Matsunami Glass, Japan), an E-beam evaporator (MHS 1800, MooHan, Korea) was used at a base pressure of 4×10^{-6} Torr. A Au layer of 40 nm was deposited onto the slide glass substrate (Figure 1B). The growth rates were manually adjusted to 1.0 Å s^{-1}. The surface of silica NPs (100 nm in diameter, Polysciences) was modified using 1% (v/v) (3-aminopropyl)triethoxysilane (γ-APTES, Sigma-Aldrich) solution in ethanol by continual stirring at RT for 24 h. The modified silica NPs were then prepared at 1% (w/v) by dispersion in ultrapure deionized (DI) water. For fabrication of multispot chips, a multispot (5 mm in diameter) silicon-rubber mask was carefully placed on the surface of the Au-deposited slide glass substrate. Then, 1 mM 4,4′-dithiodibutyric acid (DDA, Sigma-Aldrich) was introduced onto the Au-layered surface and left for 1 h to allow the formation of a self-assembled monolayer (SAM) of the DDA. The previously surface-activated silica NPs and 400 mM 1-ethyl-3-(3-dimethylaminopropyl)carbodiimide (EDC, Sigma-Aldrich) were mixed at a 1:1 ratio and introduced to the activated SAM formation for 1 h. After addition of each solution, the NP layer-modified substrates were rinsed thoroughly with ultrapure DI water to remove the excess surface-modified NPs and subsequently dried at RT (Figure 1C). Finally, a top Cu layer was deposited onto the NP layer-modified substrate using the

Table 1. Oligonucleotides Used in This Study

classification	name	length (-mer)	sequence (5′→3′)	notes
probes	Vvul02-20	20	HS-$(CH_2)_6$-GTAGTTGACGATGCATGTTC	species-specific probe for *V. vulnificus*
	Sal01	22	HS-$(CH_2)_6$-CACAAAAGCGCATGTGCTGTGA	species-specific probe for *Salmonella* spp.
	Sau001-20	20	HS-$(CH_2)_6$-CAAAGGACGACATTAGACGA	species-specific probe for *S. aureus*
	SepM02-20	20	HS-$(CH_2)_6$-TTAGGGTTCACGCCCAGAAG	species-specific probe for *S. epidermidis*
	Efa11	27	HS-$(CH_2)_6$-CATAGCTGATTAGAGGTAGACGCAGAG	species-specific probe for *E. faecalis*
	Kox1-25	25	HS-$(CH_2)_6$-ATCCGGAACGTTACTAACGCTGAGG	species-specific probe for *K. oxytoca*
primers	1585Fw	18	TTGTACACACCGCCCGTC	broad-spectrum primers
	23BR	22	TTCGCCTTTCCCTCACGGTACT	broad-spectrum primers
	MS37Fw	24	AGGATGTTGGCTTAGAAGCAGCCA	broad-spectrum primers
	MS38R	25	CCCGACAAGGAATTTCGCTACCTTA	broad-spectrum primers
	Ngo2Fw	21	AAGGGAAACCGGGTTTGTAGC	*N. gonorrhea* specific primer
	Ngo2R	23	GATGCGTCGTTATTCTACTTCGC	*N. gonorrhea* specific primer
	Ngo3R	25	TTACCTACCCGTTGACTAAGTAAGC	*N. gonorrhea* specific primer
	Ngo4R	25	CCGGGTACTTAGATGGTTCAGTTCT	*N. gonorrhea* specific primer

E-beam evaporator (Figure 1D). The surface coverage and the average number of particles per spot were determined from the scanning electron microscope (SEM) image of the MC-NPA chip surface (see Figure S1 and Table S1 in the Supporting Information). The surface coverage of nanoparticles on the spot of a MC-NPA chip was calculated following the method reported previously.[18,19] For the removal of Cu oxides generated naturally on the surface of a MC-NPA chip, the MC-NPA chips were immersed in acetic acid solution (OCI, Korea) for 20 s before use. The optical measurement system for measuring the LSPR spectra is shown in Figure S2 (see Supporting Information).

Theoretical Method for Describing Simulation Data. The reflection and extinction spectrum of a thin-film multilayer such as the MC-NPA chip could be calculated analytically. Parameters necessary for calculation are RI (N) and thickness (d) of each layer and light wavelength (λ) as shown in Figure S3, Supporting Information. First, the RI of a porous Cu film (N_e) was calculated by using Maxwell−Garnett effective medium theory.[20,21] The effective dielectric constant (ε_e (= N_e^2)) of a composite containing pores (ε_i) embedded in a host matrix (ε_m) was derived in the following equation.

$$\varepsilon_e = \varepsilon_m \frac{\varepsilon_i(1 + 2\delta) - \varepsilon_m(2\delta - 2)}{\varepsilon_m(2 + \delta) + \varepsilon_i(1 - \delta)}$$

Here, δ is the volume fraction of pores in the composite. In our case, the host matrix was the Cu layer, and the pore consists of air. Furthermore, the reflection and extinction spectrum could be calculated by using the characteristic matrix (M) of each layer.[22,23]

$$M_j = \begin{bmatrix} \cos\Delta_j & (i\sin\Delta_j)/N_j \\ iN_j\sin\Delta_j & \cos\Delta_j \end{bmatrix} (j = \text{e or } SiO_2 \text{ or Au})$$

Here, Δ_j is described as $\Delta_j = (2\pi/\lambda)N_j d_j$. The product of each matrix became a characteristic matrix of the multilayer such as (M_{multi}).

$$M_{multi} = M_e \cdot M_{SiO_2} \cdot M_{Au} = \begin{pmatrix} m_{11} & m_{12} \\ m_{21} & m_{22} \end{pmatrix}$$

The reflectance (R) for the normal incident light was calculated as follows:

$$R = \frac{(n_0 m_{11} - n_m m_{22})^2 + (n_0 n_m m_{12} - m_{21})^2}{(n_0 m_{11} + n_m m_{22})^2 + (n_0 n_m m_{12} + m_{21})^2}$$

From the above equations, the reflectance was calculated at a certain wavelength (λ). In our case, the reflectance spectrum was obtained by the change of wavelength from 400 to 750 nm at a 5 nm interval. The extinction spectrum was defined by $\log_{10} 1/R$ in this study. All calculations were conducted with a Fortran program.

Immobilization of Probe DNAs on the MC-NPA Chip. The thiolated probe DNAs (Genotech, Daejeon, Korea, Table 1) were treated with 1 M dithiothreitol and purified using a NAP-5 column (GE Healthcare). The MC-NPA chips were incubated with 1 μM probe DNAs in DI water at RT for 4 h. The chips were washed with DI water for 5 min and dried under a nitrogen stream.

Preparation and Hybridization of Target DNAs from Reference Strains and Clinical Isolates. Reference bacteria were obtained from the American Type Culture Collection (ATCC, Rockville, MD), Korean Collection for Type Cultures (KCTC, Daejeon, Korea), and Korea Culture Center of Microorganisms (KCCM, Seoul, Korea) (Table S2, Supporting Information). All clinical isolates were provided from Yonsei University College of Medicine (Korea).[24,25]

DNAs from reference bacteria were isolated using the DNA mini kit (QIAGEN, Hilden, Germany) according to the manufacturer's procedure. Clinical samples from infected patients were collected for routine culture detection, and then bacterial colonies were isolated on the plates for the identification of bacteria. DNAs from clinical isolates were extracted using the QIAamp DNA Blood Mini Kit (QIAGEN) according to the manufacturer's protocol.

PCR preparation for target DNAs was performed with the broad-spectrum and species-specific primers by using the genomic DNAs from reference bacteria and clinical isolates. PCR was performed in 50 μL reactions containing 1× *Taq* buffer, 0.2 mM dNTPs, 2 units of *Taq* polymerase (Takara Shuzo, Shiga, Japan), 5 ng of genomic DNA, 5 pM forward primer, and 25 pM reverse primer. Species-specific primers have the same sequences as those of species-specific probes. PCR using broad-spectrum

primers (1585Fw and 23BR for *Vibrio vulnificus, Salmonella* spp., *Staphylococcus aureus, Enterococcus faecalis,* and *Neisseria gonorrhea*; MS37Fw and MS38R for *Staphylococcus epidermidis* and *Klebsiella oxytoca*) was performed under the following amplification conditions: 94 °C for 4 min, followed by 35 cycles of 95 °C for 30 s, 54 °C for 30 s, and 72 °C for 1 min, and a final extension at 72 °C for 5 min. PCR using species-specific and broad-spectrum primer (23BR for *V. vulnificus, Salmonella* spp., *S. aureus, E. faecalis,* and *N. gonorrhea* and MS38R for *S. epidermidis* and *K. oxytoca*) was performed under the following amplification conditions: 94 °C for 4 min, followed by 40 cycles of 95 °C for 30 s, 52 °C for 30 s, and 72 °C for 30 s, and a final extension at 72 °C for 5 min. PCR amplicons were then purified using PCR purification kit (iNtRON, Gyeongido, Korea) according to the manufacturer's protocol. The resultant target DNAs were spotted and incubated on the MC-NPA chips at RT for 4 h. After the chips were washed with DI water for 5 min, LSPR spectra were measured under ambient conditions.

RESULTS AND DISCUSSION

Optical Characteristics of MC-NPA Chips and Cu Layer Dependence of LSPR Properties. Figure 1 shows the fabrication procedure for MC-NPA chips and the LSPR optical characteristics of each process. The excellent monodispersity of commercially available silica NPs translates directly to the uniformity of the resulting Cu NPs, which exhibit unique optical properties in the visible region. The LSPR spectrum peak position is in good agreement with that predicted by the Mie theory, and this behavior is exhibited for a variety of shell thicknesses.[15] The conventional LSPR-based nanochips require complicated procedures during the synthesis of the metal NPs with uniform size and their immobilization as a monolayer onto the solid substrate surface. However, the LSPR-based MC-NPA chip is easy to fabricate with the self-assembly of surface-functionalized silica NPs and the subsequent Cu deposition onto them.

The influence on optical characteristics by the thickness of the deposited Cu layer was investigated. On the basis of the silica NP of 100 nm in diameter, significant changes in the LSPR spectra were observed when various Cu layers with different thicknesses were deposited on the silica NP surface as shown in Figure 2. Figure 2A illustrates the experimental LSPR spectra with different thicknesses of the Cu layer on the silica NP substrates. For qualitative explanation of experimentally obtained optical spectra, we performed a calculation using the characteristic matrix method. This method is useful for the calculation of optical properties of thin-film multilayers as described elsewhere.[22,23] In the present case, the effective RI of the Cu layer deposited on the silica NPs was approximated to be that of a porous Cu film deposited on a silica layer of 100 nm and was calculated by the Maxwell−Garnett effective medium theory.[20,21] The calculations were performed for Cu thickness corresponding to actual structures. The Cu thickness dependence of optical spectra derived from the calculation agreed qualitatively with the experimental result as shown in Figure 2A and 2B. This suggests that the spectral shape of this sensor chip is mainly attributed to the interference of the thin-film multilayer structure. The Cu thickness dependence of the optical spectra was expressed in the two-dimensional (2D) color map as shown in the Figure 2C. This 2D color map demonstrates that a sharp spectral peak is observed only for a limited Cu thickness. In these measurements, deposition of a 10 nm Cu thickness on the NP surface caused the increase in the LSPR spectra due to the slight initial capping of Cu on the NP surface. However, an extremely thin film seemed to be insufficient to cover all of the silica NPs to make a uniform core−shell NP structure. The growth of the Cu layer by the metal evaporation technique caused a considerable enhancement in the extinction intensity of the LSPR spectra until the Cu reached a thickness of 30 nm. These results suggested a strong enhancement of the local electromagnetic field surrounding the core−shell NP due to the interaction of the electromagnetic radiation of incident light with the free electrons in the metal shell part. On the other hand, a deposition of Cu to a thickness over 30 nm creates vigorous contact in the shell of the closed NP and thus causes a drastic reduction in the extinction intensity and the broad bandwidths of the LSPR spectra. Consecutive incubations under ambient conditions did not nearly affect the LSPR wavelength change of these chips, which was shifted toward red as little as approximately 0.06 nm/day, indicating no discernible change of wavelength (Figure S4 in Supporting Information). The good stability of MC-NPA chips in the air under ambient conditions is thus expected to generate new opportunities for the development of reliable sensor devices for the variable sensing of biomolecules.

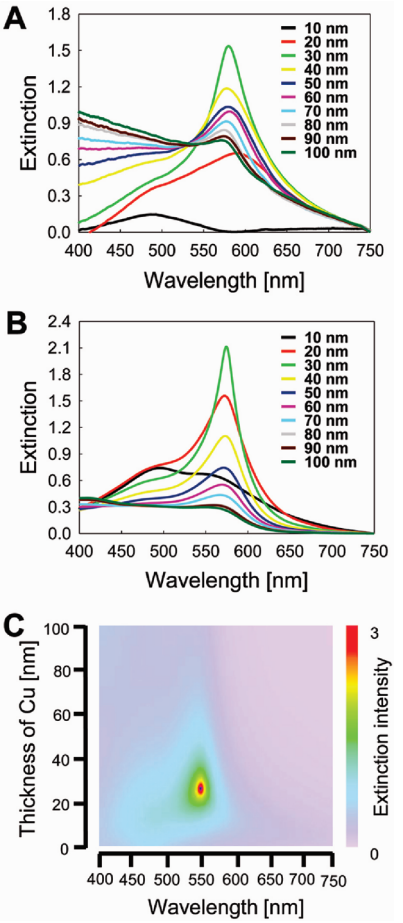

Figure 2. The LSPR properties of MC-NPA chips with surface-deposited Cu layers of various thicknesses. (A) Experimental result. (B) Simulation result. (C) 2D color map.

Sensitivity of the MC-NPA Chip to Changes in RI. To examine transduction from the surrounding RI to the LSPR spectrum, the immobilization ability of the Cu layer was tested. Figure 3 shows typical LSPR spectra of MC-NPA chips immersed in several kinds of liquid samples, such as methanol

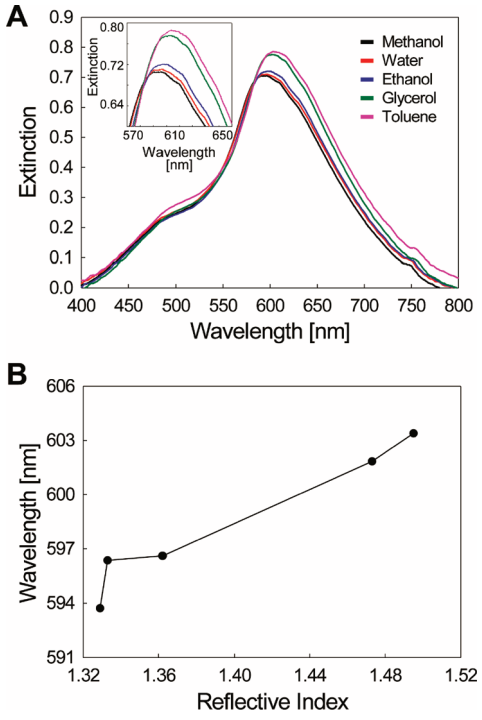

Figure 3. The LSPR spectra of the MC-NPA chip surface immersed in liquid samples of various RI in the following: methanol (n = 1.329), water (n = 1.333), ethanol (n = 1.362), glycerol (n = 1.473) and toluene (n = 1.495). The MC-NPA chip was obtained as a sensitivity of 67.8 nm RIU^{-1}. (A) Spectrum profiles of MC-NPA chip is shown in the illustrations and are magnified (inset). (B) Plot of LSPR wavelength versus RI.

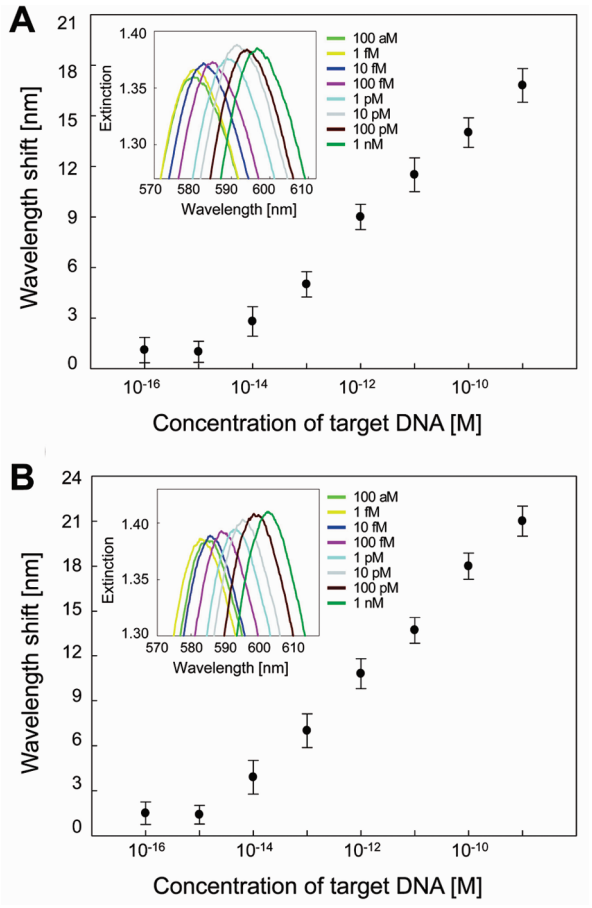

Figure 4. The detection limit of MC-NPA chips for DNA detection. Target DNAs were prepared by amplifying with broad-spectrum primers. The detection limit was determined by observing the red-shift of wavelength of chips, which were applied with different concentrations (10^{-16} to 10^{-9} M) of target DNAs from reference bacteria: (A) *S. aureus* (757-mer) and (B) *N. gonorrhea* (1236-mer). The graph of LSPR wavelength shift versus target DNA concentration shows a linearly fitted line. The data were obtained from three measurements, and the error bars represent standard deviations. The insets represent LSPR spectrum profiles of the chip.

(n = 1.329), water (n = 1.333), ethanol (n = 1.362), glycerol (n = 1.473), and toluene (n = 1.495). In these measurements, the MC-NPA chip was immersed in liquids of increasing RI, and an LSPR spectrum was recorded for each medium. The LSPR spectra of the MC-NPA chips exhibited a red shift in the LSPR spectrum peak along with an increase in the extinction at the LSPR spectrum peak as a function of the RI of the solvent in the range of 1.329−1.495, as shown in Figure 3. The MC-NPA chip gives a sensitivity of 67.8 nm RIU^{-1}. These results clearly show that the peak of an immobilized Cu layer of a MC-NPA chip is sensitive to the RI of the surrounding bulk medium. Encouraged by these results, we investigated whether the RI change at the surface of the MC-NPA chip due to biomolecular binding events could also be transduced into an experimentally detectable change in the LSPR spectra.

Optimization Conditions for Immobilization and Hybridization of DNAs on MC-NPA Chips. In order to obtain the highest performance of DNA sensing, it is important to optimize the immobilization and hybridization of DNAs on the chips. More specifically, the appropriate concentration of probes and target DNAs, incubation time, and incubation buffer needs to be chosen. Although various conditions have been studied for efficient immobilization and hybridization of DNAs on the metal-coated surface, there appeared to be no reported work on the detection of DNAs using the Cu-coated biosensor.

The optimal concentration of probe DNAs, solution, and incubation time for an efficient immobilization of the probe DNAs on the MC-NPA chips were determined to be 10 μM, 4 h, and DI water, respectively (Figures S5 and S6 in Supporting Information). For the deterimination of the optimal solution, we examined various buffer solutions such as a saline−sodium citrate (SSC), saline−sodium phosphate−EDTA buffer (SSPE), 2-(N-morpholino)ethanesulfonic acid (MES), phosphate-buffered saline (PBS), potassium dihydrogen phosphate (KH_2PO_4) buffer, phosphate buffer (PB), and DI water, which are generally used in DNA experiments. As a result, exfoliation of the Cu layer on the chip was observed upon treatment with all solutions except DI water. DI water was thus used during subsequent experiments such as an immobilization, hybridization, and washing. It is also important to determine the optimal incubation time for hybridization in which target DNAs could bind sufficiently with probe DNAs on the MC-NPA chips for the largest change of the LSPR wavelength shift. Figure S7A−C shows a representative plot of a wavelength shift obtained by applying reference bacteria to the chip. Target DNAs from three bacteria include 194-mer (A, *S. aureus*), 434-mer (B, *K. oxytoca*), and 1236-mer (C, *N. gonorrhea*), respectively. Regardless of the length of target DNA, the LSPR spectrum peaks red-shifted with

dx.doi.org/10.1021/ac2007762 |*Anal. Chem.* 2011, 83, 6215–6222

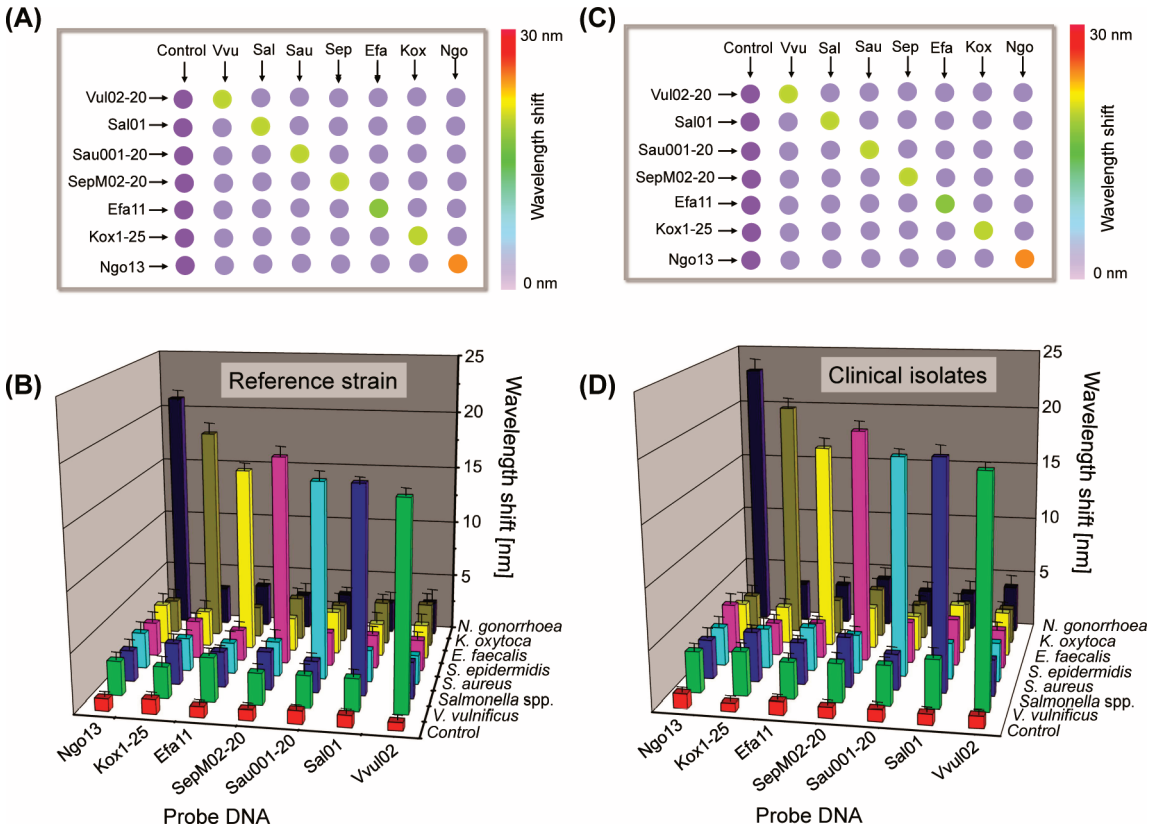

Figure 5. Affinity stringency observed from the hybridization of target DNAs amplified from reference bacteria and clinical isolates using the MC-NPA chip. Each probe DNA and target DNAs from reference strains and clinical isolates were applied to specific positions on the MC-NPA chip. The LSPR wavelength shift of each spot on the MC-NPA measured after hybridization of target DNA from reference strains and clinical isolates. The LSPR wavelength shift of each spot on the MC-NPA was represented by colorized intensity and by the bar size on the upper (A and C) and lower panels (B and D), respectively. The LSPR wavelength shift of each spot on the MC-NPA was also expressed in color (the upper part of A and B). The DI water without target DNAs was applied to the MC-NPA chip as a negative control. Abbreviations: Vvu, *V. vulnificus*; Sal, *Salmonella* spp.; Sau, *S. aureus*; Sep, *S. epidermidis*; Efa, *E. faecalis*; Kox, *K. oxytoca*; Ngo, *N. gonorrhea*.

the increased incubation time of the target DNAs and the change of the wavelength shift was saturated at 4 h. MC-NPA chips exhibit more clearly a change in the wavelength shift as the incubation time for the target DNA increases than in the extinction intensity of the peak when the probe and target DNA binds subsequently to the chip (Figure S7D in Supporting Information). Also, as the size of target DNAs increased, the LSPR wavelength was much more shifted. Thus, we investigated the relationship between target DNA length and LSPR wavelength shift in this chip.

Detection Limit of MC-NPA Chip. A large change in the wavelength shift upon hybridization of target DNAs could be an indication of a detection limit of very small concentrations by the sensor chips. Especially, chips showing a large change in wavelength indicate that they are sensitive to small amounts of target DNAs. Figure S8 (Supporting Information) shows the detection limit of MC-NPA chips for DNA detection by observing the red-shift of the wavelength as a function of the concentration of target DNAs (10^{-15} to 10^{-6} M). The target DNAs from reference strains were prepared by amplification with a species-specific primer and a broad-ranged primer (see Experimental Section) and had various lengths ranging from 119- to 1236-mer. As expected, the incubation of target DNAs having different sizes gave different detection limits for the chip. For example, the detection limit for the chip is 1 pM when applied to target DNAs from *V. vulnificus* (119-mer), *Salmonella* spp. (138-mer), *S. aureus* (194-mer), and *S. epidermidis* (202-mer) in a typical assay volume of 5 μL. The target DNAs from *E. faecalis* (353-mer) and *K. oxytoca* (434-mer) showed a 100 fM detection limit. Remarkably, target DNA from *N. gonorrhea* (1236-mer), which displays the largest change in wavelength shift could lower the detection limit to 10 fM (Figure S8 in Supporting Information). In addition, a stable, quantitative, and reproducible signal from the chip was obtained by applying a target DNA concentration between 10^{-14} and 10^{-9} M. On the basis of this result, we further applied long target DNAs of all bacteria by amplifying with broad-spectrum primers (see Experimental Section, Table 1) and determined the detection limit of this assay (Figure 4, and Figure S9 in Supporting Information). The lengths of target DNAs from seven bacteria were as follows: 772-mer for *V. vulnificus*, 791-mer for *Salmonella* spp., 757-mer for *S. aureus*, 879-mer for *S. epidermidis*, 712-mer for *E. faecalis*, 900-mer for *K. oxytoca*, and 1236-mer for *N. gonorrhea*. The use of broad-spectrum primers for target DNA preparation provides the amplification of the target DNAs from any bacterial species in samples and thus also produces an incredibly sensitive result for identifying unknowns, compared with the use of multiplex primers which can produce poor sensitivity and specificity.[26] It is important to determine the target DNA length because an excessively long target DNA can reduce LSPR wavelength shift and reproducibility because of its

dx.doi.org/10.1021/ac2007762 |*Anal. Chem.* 2011, 83, 6215–6222

secondary structure and poor hybridization between DNAs.[9] The broad-spectrum primers were selected for high signal intensities and specificity in a previous study.[27] As a result, the chip applied to long target DNAs showed ultrasensitive sensing performance. The detection limit for this chip was 10 fM when applied to all long target DNAs from seven target pathogenic bacteria (Figure 4, and Figure S9 in Supporting Information). This value corresponds to 50 zmol (3×10^4 molecules) in a 5 μL sample volume. Although some assays require an additional step, design of modified probes, or reaction catalysts such as enzymes (femtomolar detection limit), this method is very simple and sensitive, with a detection limit close to or lower than that of signal amplification strategies that are combined with detection assays.[28−31] Thus, the sensitivity of this assay can be more enhanced by combining the amplification-based and target recycling reaction. Considering that one of the major challenges for a pathogen-diagnostic assay lies in the sensitive detection of bacterial DNAs, especially DNAs with long length, this result is quite impressive and represents the practicality of this method in various fields including DNA sensing. This ultrasensitive sensing performance of MC-MPA chips makes them obvious, promising platforms as a diverse sensing device in clinical diagnostics.

Specificity of the MC-NPA Chip. For the accurate identification of multiple pathogenic bacterial DNAs, the capacity for highly selective DNA hybridization by the MC-NPA chip is needed. Figure 5A shows the wavelength shift of the LSPR peak after the application of target DNAs derived from seven reference bacteria. The red-shift of the LSPR wavelength after subsequent hybridization revealed that target DNAs amplified from these bacteria hybridized strongly to probes derived from their respective sequences. On the other hand, the interaction between the probe DNA and target DNA amplified from other species showed a discernible change in wavelength shift. This result suggests that the present system can discriminate the sequence-specific DNA hybridization without cross-reactivity and nonspecific adsorption.

Validation of Practical Usefulness of the MC-NPA Chip Using Clinical Isolates. To assess the performance of the MC-NPA chip in a clinical setting, seven blind samples from various clinical specimens including blood, pus, sputum, and urine were tested. The results were compared with those obtained using culture-based assays (Figure 5B). The LSPR-based assay correctly identified seven clinical isolates. These results indicate that the MC-NPA chip developed in this study allows successful diagnosis of a range of pathogenic bacteria from various clinical samples.

The MC-NPA chip provides a convenient and label-free method for specific and highly sensitive detection of the biomolecular interactions in a parallel format as shown in Figure 5. Furthermore, different from the fabrication of Cu NPs and Cu nanocrystals in solution, Cu-capped NP structures developed here are easy to fabricate and to control in various platforms with high reproducibility. From a practical and commercial point of view, it is valuable to employ Cu nanoshells as nanostructures for potential large-scale or large-area applications currently being conducted with Au and Ag because of the significantly reduced relative cost of the constituent metal. We anticipate that this technology will extend the limits of current molecular diagnostics and enable point-of-care diagnosis as well as promote the development of personalized medicine. The multiparallel possibilities of biosensing applications have the potential to allow the optimization of biomarker research, cancer diagnosis, and also the detection of infectious microorganisms for biodefense.

CONCLUSIONS

The high sensitivity of the MC-NPA chip with respect to analyte concentration enables the quantification of biomolecules in small volumes in a rapid and simple format. Cu metal is unstable, difficult to work with, and prone to surface oxidation that can significantly affect the optical properties. However, we obviously examined the plasmonic properties of the Cu-based core−shell nanostructure throughout the visible region with the control of the shell thickness of the deposited Cu layer, indicating that the instability and difficulty in working with Cu is not a problem with our method. Also, we investigated the ability of the Cu layer to transduce changes in the surrounding RI into the LSPR spectrum. These results could be obtained by the Cu oxide removal procedure on the surface of MC-NPA chip. In this research, the LSPR-based optical biosensor constructed with the MC-NPA chip was applied to label-free detection of bacterial DNA hybridization. This is the first report on the monitoring of biomolecular interaction by using a dense NP array chip based on the Cu metal substrate. As a result, the MC-NPA chip led to a discovery that the detection limits of target DNAs were approximately 10 fM (50 zmol) in specific tests using four untagged DNA samples from reference bacteria and clinical isolates. Experiments with clinically important bacteria-specific DNA samples directed toward this goal are currently in progress in our laboratory. Furthermore, these results demonstrate that MC-NPA chips developed can be used for various DNA sensing applications such as disease diagnostics.

ASSOCIATED CONTENT

Supporting Information. Additional information as noted in the text. This material is available free of charge via the Internet at http://pubs.acs.org.

AUTHOR INFORMATION

Corresponding Author

*Phone: +82-42-350-3930. Fax: +82-42-350-8800. E-mail: leesy@kaist.ac.kr (S.Y.L); tjpark@kaist.ac.kr (T.J.P).

ACKNOWLEDGMENT

This work was supported by a grant from the National Fisheries Research and Development Institute (NFRDI), Republic of Korea. D.-K.K. and S.M.Y. contributed equally to this work.

REFERENCES

(1) Kelly, K. L.; Coronado, E.; Zhao, L. L.; Schatz, G. C. *J. Phys. Chem. B* **2003**, *107*, 668–677.

(2) Miller, M. M.; Lazarides, A. A. *J. Phys. Chem. B* **2005**, *109*, 21556–21565.

(3) Prodan, E.; Nordlander, P.; Halas, N. J. *Nano Lett.* **2003**, *3*, 1411–1415.

(4) Okamoto, T.; Yamaguchi, I; Kobayashi, T. *Opt. Lett.* **2000**, *25*, 372–374.

(5) Nath, N.; Chilkoti, A. A. *Anal. Chem.* **2002**, *74*, 504–509.

(6) Yoo, S. Y.; Kim, T.-I.; Lee, S. Y.; Kim, E. K.; Keum, K. C.; Yoo, N. C.; Yoo, W. M. *Br. J. Ophthalmol.* **2007**, *91*, 722–727.

(7) Taylor, C. J.; Bain, L. A.; Richardson, D. J.; Spiro, S.; Russell, D. A. *Anal. Biochem.* **2004**, *328*, 60–66.

(8) Oldenburg, S. J.; Averitt, R. D.; Westcott, S. L.; Halas, N. J. *Chem. Phys. Lett.* **1998**, *288*, 243–247.

(9) Endo, T.; Kerman, K.; Nagatani, N.; Hiepa, H. M.; Kim, D.-K.; Yonezawa, Y.; Nakano, K.; Tamiya, E. *Anal. Chem.* **2006**, *78*, 6465–6475.
(10) Hiep, H. M.; Endo, T.; Saito, M.; Chikae, M.; Kim, D.-K.; Yamamura, S.; Takamura, Y.; Tamiya, E. *Anal. Chem.* **2008**, *80*, 1859–1864.
(11) Yoo, S. Y.; Kim, D.-K.; Park, T. J.; Kim, E. K.; Tamiya, E.; Lee, S. Y. *Anal. Chem.* **2010**, *82*, 1349–1357.
(12) Nadagouda, M. N.; Varma, R. S. *Cryst. Growth Des.* **2007**, *7*, 2582–2587.
(13) Yang, L.-B.; Chen, G.-Y.; Wang, J.; Wang, T.-T.; Li, M.-Q.; Liu, J.-H. *J. Mater. Chem.* **2009**, *19*, 6849–6856.
(14) Wang, C.; Peng, S.; Chan, R.; Sun, S. *Small* **2009**, *5*, 567–570.
(15) Wang, H.; Tam, F.; Grady, N. K.; Halas, N. J. *J. Phys. Chem. B* **2005**, *109*, 18218–18222.
(16) Singh, M.; Sinha, I.; Premkumar, M.; Singh, A. K.; Mandal, R. K. *Colloid. Surf. A* **2010**, *359*, 88–94.
(17) Chan, G. H.; Zhao, J.; Hicks, E. H.; Schatz, G. C.; Van Duyne, R. P. *Nano Lett.* **2007**, *7*, 1947–1952.
(18) Yoo, S. Y.; Kim, D.-K.; Park, T. J.; Kim, E. K.; Tamiya, E.; Lee, S. Y. *Anal. Chem.* **2010**, *82*, 1349–1357.
(19) Stakenborg, T.; Peeters, S.; Reekmans, G.; Laureyn, W.; Jans, H.; Borghs, G.; Imberechts, H. *J. Nanopart. Res.* **2008**, *10*, 143–152.
(20) Kreibig, U.; Vollmer, M. *Optical Properties of Metal Clusters*; Springer-Verlag: Heidelberg, 1995; Vol. 25.
(21) McMillan, B. G.; Berlouis, L. E. A.; Cruickshank, F. R.; Brevet, P. F. *J. Electroanal. Chem.* **2007**, *599*, 177–182.
(22) Macleod, H. A. *Thin-Film Optical Filters*; Macmillan: New York, 1986.
(23) Palik, E. D. *Handbook of Optical Constants of Solids*; Academic Press: Orlando, FL, 1985.
(24) Yoo, S. M.; Lee, S. Y.; Chang, K. H.; Yoo, S. Y.; Yoo, N. C.; Keum, K. C.; Yoo, W. M.; Kim, J. M.; Choi, J. Y. *Mol. Cell. Probes* **2009**, *23*, 171–177.
(25) Yoo, S. M.; Choi, J. Y.; Yun, J. K.; Choi, J. K.; Shin, S. Y.; Lee, K.; Kim, J. M.; Lee, S. Y. *Mol. Cell. Probes* **2010**, *24*, 44–52.
(26) Polz, M. F.; Cavanaugh, C. M. *Appl. Environ. Microbiol.* **1998**, *64*, 3724–3730.
(27) Keum, K. C.; Yoo, S. M.; Lee, S. Y.; Chang, K. H.; Yoo, N. C.; Yoo, W. M.; Kim, J. M.; Choi, J. Y.; Kim, J. S.; Lee, G. *Mol. Cell. Probes* **2006**, *20*, 42–50.
(28) Zhang, J.; Song, S.; Zhang, L.; Wang, L.; Wu, H.; Pan, D.; Fan, C. J. *J. Am. Chem. Soc.* **2006**, *128*, 8575–8580.
(29) Zhang, Y.; Tang, Z.; Wang, J.; Wu, H.; Maham, A.; Lin, Y. *Anal. Chem.* **2010**, *82*, 6440–6446.
(30) Huang, J.; Wu, Y.; Chen, Y.; Zhu, Z.; Yang, X.; Yang, C. J.; Wang, K.; Tan, W. *Angew. Chem., Int. Ed.* **2011**, *50*, 401–404.
(31) Ferapontova, E. E.; Hansen, M. N.; Saunders, A. M.; Shipovskov, S.; Sutherland, D. S.; Gothelf, K. V. *Chem. Commun.* **2010**, *46*, 1836–1838.